FULL PAPER

Biorealistic Implementation of Synaptic Functions with Oxide Memristors through Internal Ionic Dynamics

*Chao Du, Wen Ma, Ting Chang, Patrick Sheridan, and Wei D. Lu**

Memristors have attracted broad interest as a promising candidate for future memory and computing applications. Particularly, it is believed that memristors can effectively implement synaptic functions and enable efficient neuromorphic systems. Most previous studies, however, focus on implementing specific synaptic learning rules by carefully engineering external programming parameters instead of focusing on emulating the internal cause that leads to the apparent learning rules. Here, it is shown that by taking advantage of the different time scales of internal oxygen vacancy (V_O) dynamics in an oxide-based memristor, diverse synaptic functions at different time scales can be implemented naturally. Mathematically, the device can be effectively modeled as a second-order memristor with a simple set of equations including multiple state variables. Not only is this approach more biorealistic and easier to implement, by focusing on the fundamental driving mechanisms it allows the development of complete theoretical and experimental frameworks for biologically inspired computing systems.

1. Introduction

Memristors are two-terminal electrical devices whose states are described by internal state variables and governed by dynamic ionic processes. The concept of memristors was initially proposed in the 1970s[1,2] and has been intensively investigated in the last few years.[3–7] The key advantages of memristor devices include the compact two-terminal structure, internal memory, fast speed, low power, complementray metal oxide semiconductor (CMOS) compatibility, and the ability for hybrid and 3D integration, making them attractive for a broad range of applications including memory, analog and reconfigurable circuits, as well as neuromorphic computing.[8–11]

In particular, the prospect of building biologically inspired neuromorphic computing systems with memristor-based synapses has generated significant interest.[12–14] These systems offer distributed computation and localized memory and could offer much higher capability and efficiency than today's digital computers to handle complex tasks.[13,15] To date, several studies have demonstrated basic synaptic learning rules such as spike-timing-dependent plasticity (STDP) using various types of memristors.[12,16–21] However, in these studies, the synaptic learning rules were implemented phenomenologically by engineering the duration or amplitude of the overlapping programming pulses from the pre- and postsynaptic neurons.[12,18–22] The phenomenological nature of this approach means that different programming pulses have to be manually designed to implement the desired synaptic behaviors. However, in biology, the apparently different learning rules have been shown to be specific effects driven by internal molecular dynamic processes under stimulation.[23–25] Consequently, manually designing a system to specifically target only certain effects, but not their cause, can easily miss other important aspects that make the system functional.

In a previous study, we showed that by employing multiple internal state variables (e.g., temperature and conduction filament size), a second-order memristor can be obtained which allows biorealistic implementation of several synaptic learning rules—notably spike-timing-dependent plasticity.[26] Here, we show that a second-order memristor can also be implemented by utilizing the different time scales of internal ionic dynamics in oxide-based memristors, leading to the natural implementation of several types of important synaptic behaviors. We show that an oxide-based memristor may be described by two state variables—one (w_c) directly determines the device conductance (weight) and the other (w_m) affects the dynamics of the first (conductance) state variable. Specifically in our device system, w_c represents the area of the conducting channel region in the oxide memristor thus directly affecting the device conductance, while w_m represents the oxygen vacancy mobility in the film which directly affects the dynamics of w_c but only indirectly modulates the device conductance. Within this second-order memristor framework, the device long-term state can be shown to be controlled by activities at much shorter time scales. Specifically, the natural decay of the state variable w_m provides an internal timing and modulation mechanism analogous to that exhibited by Ca^{2+} concentration,[23–25] and enables the memristor to exhibit important rate- and timing-dependent behaviors at both short-term such as pair-pulse facilitation (PPF)[27] and long-term such as STDP[28] using simple, nonoverlapping spike signals. The experimental observations can in turn be quantitatively explained using a simple dynamic device model including the two state variables, and facilitates large-scale simulation and implementation of memristor-based neuromorphic systems.

C. Du, W. Ma, Dr. T. Chang, P. Sheridan, Prof. W. D. Lu
Department of Electrical Engineering and Computer Science
University of Michigan
Ann Arbor, MI 48109, USA
E-mail: wluee@eecs.umich.edu

DOI: 10.1002/adfm.201501427

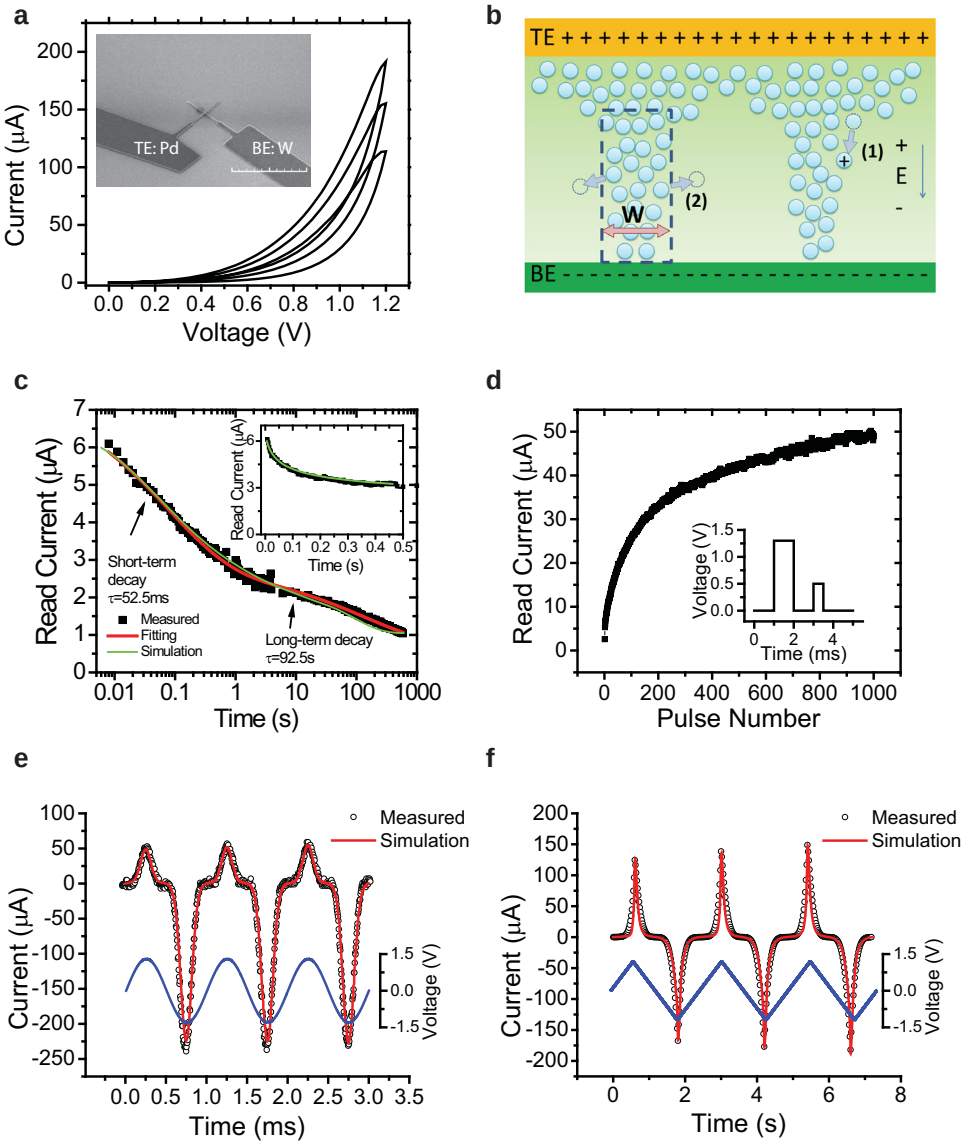

Figure 1. Electrical characterization and modeling of the memristor. a) DC characteristics of the device showing pinched hysteresis and gradual conductance increase. Three consecutive DC sweeps were applied from 0 to 1.2 V with 2 V s^{-1} ramp rate. Inset: Scanning electron microscope image of a typical device. Scale bar: 20 μm. b) Schematic illustration of the internal V_O dynamics showing: (1) electric field driven V_O drift and (2) spontaneous diffusion. c) Memristor conductance decay. The device was stimulated with ten write pulses (1.2 V, 1 ms) and the conductance decay was monitored after the stimulation. The experimental data (black squares) can be fitted by the sum of two stretched exponential functions with distinct relaxation time constants (red line). Green line shows simulation results from the memristor model (Equations (2)–(4)) that also captures the memristor behavior at different time scales. Inset: Experimental (black squares) and simulation results from the memristor model (green line) showing the memristor conductance decay plotted in linear time scale. d) Memristor conductance as a function of repeated stimulation, showing a saturation behavior. Inset: The programming waveform with a write pulse (1.3 V, 1 ms) followed by a read pulse (0.5 V, 500 μs). The device was subjected to 1000 such pulses with a repetition frequency of 50 Hz. Modeling results (solid red lines) and measured data (open circles) of the device when subjected to e) AC stimulation and f) DC stimulation. The insets show the stimulation waveforms (blue lines) corresponding to a 1 kHz sine wave with e) V_{peak} = 1.3 V and a triangular waveform with f) V_{peak} = 1.2 V and 2 V s^{-1} ramp rate.

2. Results and Discussion

2.1. Device Characteristic and Modeling

The memristor devices used in this study are based on a metal–insulator–metal (MIM) structure similar to those reported earlier.[16,17] The device has a palladium (Pd) top electrode, a tungsten oxide (WO_x) switching layer, and a tungsten (W) bottom electrode (Supporting Information). As with all memristor devices, a "pinched-hysteresis" behavior can be distinctively observed in the *I–V* characteristics as presented in **Figure 1**a. When a positive voltage is applied, the device conductance gradually increases (termed the write process) and when a negative voltage is applied the conductance gradually decreases (termed the erase process).

The conductance change can be explained by the redistribution of ions,[16,29] here in the form of oxygen vacancies, as schematically illustrated in Figure 1b. The regions rich with oxygen vacancies form high conductance channels while the rest of the regions remain at low conductance and form a Schottky contact with the W electrode. Therefore, the device can be modeled as having two conduction paths in parallel, with a state variable w_c representing the relative area of the conducting region,[16,30] as shown in Figure 1b. Specifically, we note that the V_O movement can be caused by both the electric field during programming[31] and by spontaneous diffusion,[16] also schematically illustrated in Figure 1b. These internal ionic dynamic processes allow the memristor to exhibit a number of key synaptic behaviors at short-term and long-term discussed below.

The synaptic cleft is a region between the axon of a presynaptic neuron and the dendrite of a postsynaptic neuron.[32] Spikes, or action potentials (APs) from the presynaptic neuron can be transmitted through the synapse and generate a postsynaptic potential (PSP) whose amplitude is determined by the connection strength, i.e., the synaptic weight. Here, the synaptic weight will be emulated by the conductance of the memristor. In neurobiological studies, the modulation of the synaptic efficacy (weight) can be further traced to internal molecular dynamics, e.g., modulations of the pre- or postsynaptic Ca^{2+} ion concentrations[24,25,27,33] which inspired us to explore how internal ionic dynamics in memristors can affect its conductance change. The time scales of the ionic dynamic processes can be probed by monitoring how the memristor weight evolves after stimulation, as shown in Figure 1c. In this study, ten positive write pulses (1.2 V, 1 ms) at 5 ms intervals were applied first, followed by small read pulses (0.4 V, 1 ms) to track the memristor conductance (weight) change. The stimulation drives the memristor conductance higher, however after stimulation is stopped the memristor conductance decays, likely due to the diffusion of V_O[16,21,34–36] as shown in Figure 1c. Significantly, careful analysis of the data shows that the decay appears to occur at two very different time scales: right after stimulation, the memristor conductance shows a very fast decay and the decay becomes much slower after a few hundreds of milliseconds. Specifically, the data can be well fitted with two time constants: a short-term effect with time constant ≈52.5 ms and a long-term time constant ≈92.5 s

$$I = A_1 \times I_{\text{short}} + A_2 \times I_{\text{long}} = A_1 I_{0s} \exp\left[-\left(\frac{t}{\tau_s}\right)^{\beta_s}\right] + A_2 I_{0l} \exp\left[-\left(\frac{t}{\tau_l}\right)^{\beta_l}\right] \quad (1)$$

Here, stretched exponential functions that describe relaxation in a disordered system are used to model both the short-term and the long-term decays, where τ_s (τ_l), I_{0s} (I_{0l}), β_s (β_l) are the characteristic relaxation time, prefactor, and the stretch index for the short-term (long-term term) process, respectively. Experimentally, this behavior can be explained by the fact that the state variable governing memristor conductance (w_c) is affected by how mobile the oxygen vacancies are. It has been found that the mobility of oxygen vacancies (ions) increases when they are driven out of equilibrium right after a stimulation pulse, possibly due to the local lattice distortion and strain, followed by slow relaxation after the stimulation is removed.[36] The temporary higher mobility, represented by another state variable w_m in our model, may explain the initial fast decay of the memristor conductance and also affect how the conductance state variable w_c responds to stimulation. Physically, the migration of oxygen vacancies are driven by electrochemical gradients,[37] including the field-driven drift process by an electrical potential gradient and the diffusion process driven by an internal chemical potential gradient. Additional factors (e.g., protons provided by moisture; local morphology, etc.) can in turn affect the dynamics of such processes. The formation of (electro) chemical potential gradients in both electrochemical metallization memory (ECM) and valence change memory (VCM, to which the WO_x memristor belongs) and the relaxation that lead to the experimentally observed nanobattery effect[37] have been extensively discussed previously.[37]

Borrowing terms used in neuroscience, the first stage with time constant ≈52.5 ms is considered short-term and the second stage with time constant ≈92.5 s (i.e., >1000× longer) is considered long-term. We note that even though the absolute values of the short-term and long-term characteristic time constants are different from those reported in biological synapses (e.g., tens of milliseconds to a few minutes for short-term[27] and minutes to hour for long-term,[38] the separation of the two time scales that differ by more than three orders of magnitude is evident in the memristor, and that circuits based on memristors can potentially operate at higher clock frequency (e.g., kHz or higher compared to ≈Hz in biological systems) to utilize the different dynamics in the two regimes.

Another property of the memristor device is the nonlinear response to programming. For example, in an experiment shown in Figure 1d, continuous positive write pulses (1.3 V, 1 ms) were applied to the device at a repetition frequency of 50 Hz, and the device conductance was measured by a small read pulse (0.5 V, 500 μs) after each write pulse. The read current increases quickly following the first few write pulses but gradually saturates as the device conductance increases with an increasing number of write pulses. The loss of programming capability at high conductance states is likely due to the exhaustion of the limited supply of oxygen vacancies in the switching layer.

These ionic dynamics can be captured in a memristor model considering two state variables

$$I = (1 - w_c) \times \alpha \times \left[1 - \exp(-\beta V)\right] + w_c \times \gamma \times \sinh(kV) \quad (2)$$

$$\frac{dw_m}{dt} = \lambda_m W(w_m, V) \sinh(\rho_m |V|) - \frac{w_m - w_{m0}}{\tau_m^*(w_m)} \quad (3)$$

$$\frac{dw_c}{dt} = \lambda_c W(w_c, V) \exp(\varepsilon w_m) \sinh(\rho_c V) - \frac{w_c - w_{c0}}{\tau_c^*(w_m)} \quad (4)$$

Here, Equation (2) is the current–voltage equation determined by the state variable w_c, which represents the effective area of the conducting region, as discussed in previous studies.[16,30] Equations (3) and (4) are the dynamic equations of the two state variables w_m and w_c, in which the first term describes

the effect of the stimulation voltage, while the second term describes the effect of decay with effective time constants (τ_m^* and τ_c^*). Specifically, the dynamic Equation (3) for state variable w_m, which represents the effective mobility of the V_Os, shows that the V_Os become more mobile with stimulation since more V_Os are driven out of equilibrium, and the mobility enhancement fades after stimulation is removed.[36] Additionally, w_m affects how w_c changes with stimulation through the factor $\exp(\varepsilon w_m)$ in Equation (4). The decay of w_c may also be affected by the V_O mobility so the effective decay time constant τ_c^* is considered a function of w_m too. In this sense, the memristor can be considered as a "second-order" memristor[26,39] where the state variable that directly controls the device current–voltage characteristics, w_c, is modulated by another state variable w_m. In particular, even though the enhancement of w_m is mostly short-term with an effective time constant of only 10 s of milliseconds, it can (indirectly through Equation (4) have long-term effects on the device conductance. The values of the device-specific parameters and the choice of the "window function" $W(w,V)$ that reflects the nonlinear state-dependent programming capability and the effective time constant functions $\tau_m^*(w_m)$ and $\tau_c^*(w_m)$ can be found in the Supporting Information.

This memristor model based on two state variables can quantitatively capture the ionic dynamics and describe the device response over a large range of programming conditions. For example, the two-stage decay phenomenon can be well-reproduced through simulation based on Equations (2)–(4) (Figure 1c). Simulation results based on this dynamic model can also quantitatively explain both the AC (Figure 1e) and DC (Figure 1f) responses of the device.

Below we show that the internal ionic dynamics of the memristors can be used to natively emulate a diverse range of synaptic behaviors at both short-term such as PPF[27] and long-term such as STDP[28] using simple spike signals, without having to engineer arbitrary, overlapping pulses. Unlike our previous study that relies on temperature as the second state variable[26] and requires a separate heating pulse to initiate the temperature change, here both state variables are associated with the same specie (oxygen vacancy) and can be excited by using a single, simple (e.g., square) pulse. Additionally, these experimental results can be fully explained by the memristor model based on the two state variables, using essentially a single set of material-dependent parameters (Supporting Information).

2.2. Paired-Pulse Facilitation

Paired-pulse facilitation (PPF) is an important short-term phenomenon extensively discussed in neuroscience studies.[27] PPF states that when two excitatory presynaptic spikes are applied successively, the second spike will generate a larger excitatory postsynaptic current (EPSC) than the first pulse. Additionally, the amplitude of EPSC caused by the second pulse is determined by the time interval between the two pulses and a larger interval will lead to a smaller EPSC amplitude enhancement. Results from studies on guinea pig hippocampal cells are reproduced in **Figure 2**a.[40] The PPF effect is believed to be caused by the residual Ca^{2+} concentration in the presynaptic neuron induced by the first spike which enhances the overall Ca^{2+} level and the resulting EPSC generated by the second spike. Due to the exponential decay of the residual Ca^{2+} caused by the first spike, the effect naturally becomes weaker when the interval between the two spikes increases.[27]

Figure 2b shows similar effects obtained in the memristor device when applied with two identical, nonoverlapping pulses. Similar to PPF studies in biology, the intervals between the two write pulses (simple square pulses with amplitude of 1.4 V and duration of 1 ms) were changed systemically to probe how the memristor responds to the paired pulses. First, we notice that the current spike through the memristor during the second voltage pulse is indeed larger than that during the first pulse, similar to PPF effects. Analogous to the residual effects of Ca^{2+} in biological synapses, the enhancement in programming current (determined by w_c) observed in the second pulse can be explained by the residual mobility enhancement effect (represented by w_m) from the first pulse. If the second pulse is applied before w_m has decayed to its resting value, an enhanced current spike will be obtained, as expected from PPF effects. Additionally, with increasing interval between the two pulses, the enhancement is reduced (Figure 2b), as the enhanced w_m gradually decays toward its resting value.

The PPF effect observed in memristors can be better illustrated by calculating the conductance change by comparing the device conductance measured immediately after the first pulse (p_1) and the second pulse (p_2). The dependence of the conductance enhancement on the pulse interval (Figure 2c) again shows a similar trend to that observed in biological systems (Figure 2a). A larger interval will lead to a smaller conductance enhancement and this could be directly explained from the perspective of the enhancement and decay of the state variable w_m, as discussed above. Specifically, the change in device conductance as a function of pulse interval can be quantitatively explained through simulations based on the device model, shown as the solid line in Figure 2c.

As an extension of PPF, if more than two excitatory presynaptic spikes are applied to the synapse, the amplitude of the resulting EPSC will continue increasing gradually. The extent of the synaptic weight change depends on the frequency of stimuli, which is inversely related to the interval between each pulse. To verify that the internal V_O dynamics can naturally lead to similar frequency-dependent weight change, we applied ten continuous write pulses (1.25 V, 1 ms) with different frequencies and monitored the current during each pulse (Figure 2d). The device current was indeed found to increase gradually, and, more interestingly, at different rates depending on the stimulation frequency. The increase in current, measured at the last pulse and compared to the first pulse, is calculated and shown in Figure 2d. A clear trend in the potentiation effect with respect to the stimulation frequency can be observed. As the stimulation frequency increases, the increase in current is more significant. This frequency dependence can be readily explained using the V_O dynamics following the residual calcium concentration model, as pulse trains with higher frequency mean smaller intervals between pulses to allow w_m decay and result in more effective accumulation of the V_O, as already explained in the PPF experiments. Again the experimental data can be

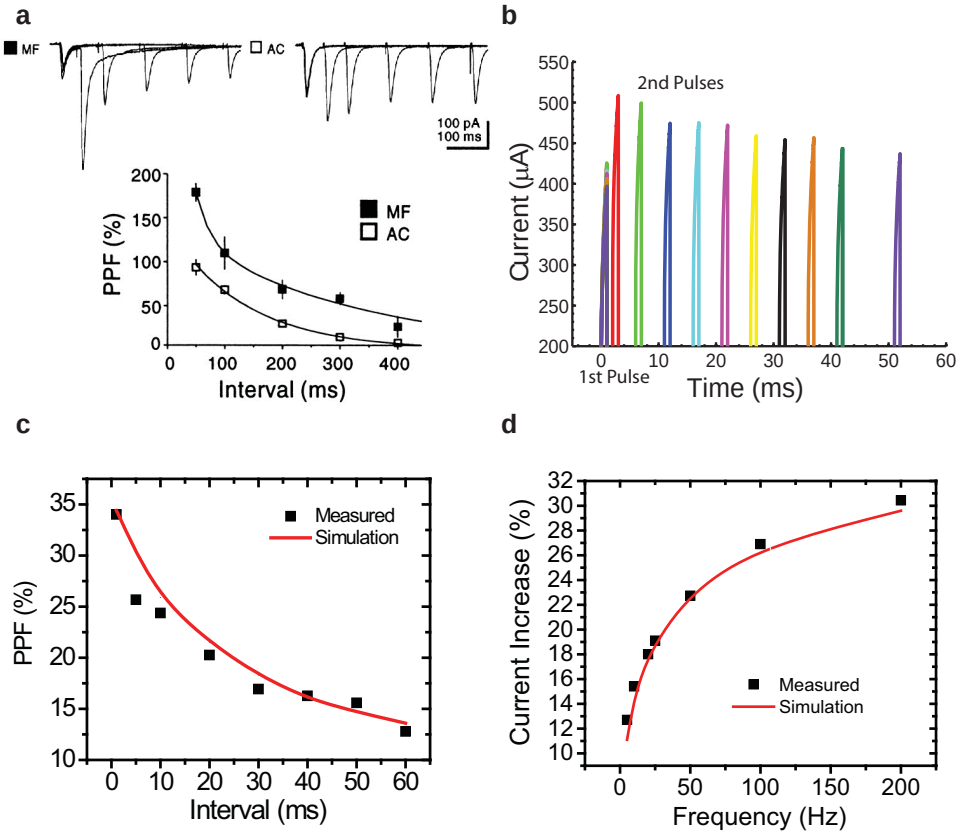

Figure 2. Paired-pulse facilitation effect in memristors. a) Results of PPF from mossy fiber (MF) and assoc/com (AC) synapses. Adapted with permission from ref. [40]. Top: EPSP obtained from paired pulses with different intervals. The EPSP from the second pulse is enhanced, and the enhancement is weaker with longer intervals between the pulses. Bottom: PPF ratio as a function of pulse interval. The ratio was defined as $(p_2 - p_1)/p_1$, where p_1 and p_2 are the amplitude of the EPSCs evoked by the first and second pulse, respectively. b) PPF effect obtained in the memristor by applying two paired pulses (1.4 V, 1 ms) at ten different intervals. The second pulse produces an enhanced response in all cases, and increasing the pulse interval leads to a decrease in the enhancement. c) PPF ratio as a function of pulse interval, showing a similar trend to (a). Squares: Experimental data. Line: Simulation results from the memristor model using experimental parameters. d) Change in memristor current after the application of pulse trains consisting of ten write pulses (1.25 V,1 ms) with different frequencies. Higher stimulation frequency leads to larger conductance enhancement. Squares: Experimental data. Line: Simulation results from the memristor model using experimental parameters.

quantitatively explained by the memristor model (solid line in Figure 2d).

2.3. Experience-Dependent Plasticity

Another important synaptic behavior is that the synaptic plasticity is experience dependent. For example, according to Bienenstock, Cooper, and Munro (BCM),[41] the synapse can exhibit either potentiation (synaptic weight strengthening) or depression (synaptic weight weakening) even when subjected to the same spike trains. In other words, not only the amplitude but also the sign of synaptic weight change depends on the present stimulation conditions as well as the stimulation history. Specifically, Bear et al.[42] found that high frequency stimulation normally leads to potentiation and low frequency stimulation normally leads to depression, and there exists a threshold frequency at which the synaptic weight can be maintained. Additionally, the threshold frequency will also shift accordingly, depending on the experience of the synapse.[42] For example, after a period of increased synaptic activity, the threshold will slide to right (higher frequency), promoting synaptic depression such that spike trains that previously caused potentiation may now be below the threshold frequency and will cause depression instead. Similarly, after a period of decreased activity, the threshold will slide to left, promoting synaptic potentiation and it will be easier to enhance synaptic weight with lower-frequency spikes. The sliding threshold effect from Bear's study[42] on visual cortex is reproduced in **Figure 3**a.

In our experiment, we applied a series of pulse trains, each consisting of five identical programming pulses (1 V, 1 ms), with different frequencies and recorded the memristor conductance change as shown in Figure 3b. In step 1, the first pulse train with a 200 Hz stimulation frequency was applied and resulted in an increase in current through the memristor. Subsequently, in step 2, a 10 Hz pulse train caused the memristor current to drop. On the other hand, following the 1 Hz pulse train in step 3, the same 10 Hz pulse train in step 4 created an increase in memristor current instead. The sign reversal with respect to current change at the same 10 Hz stimulation

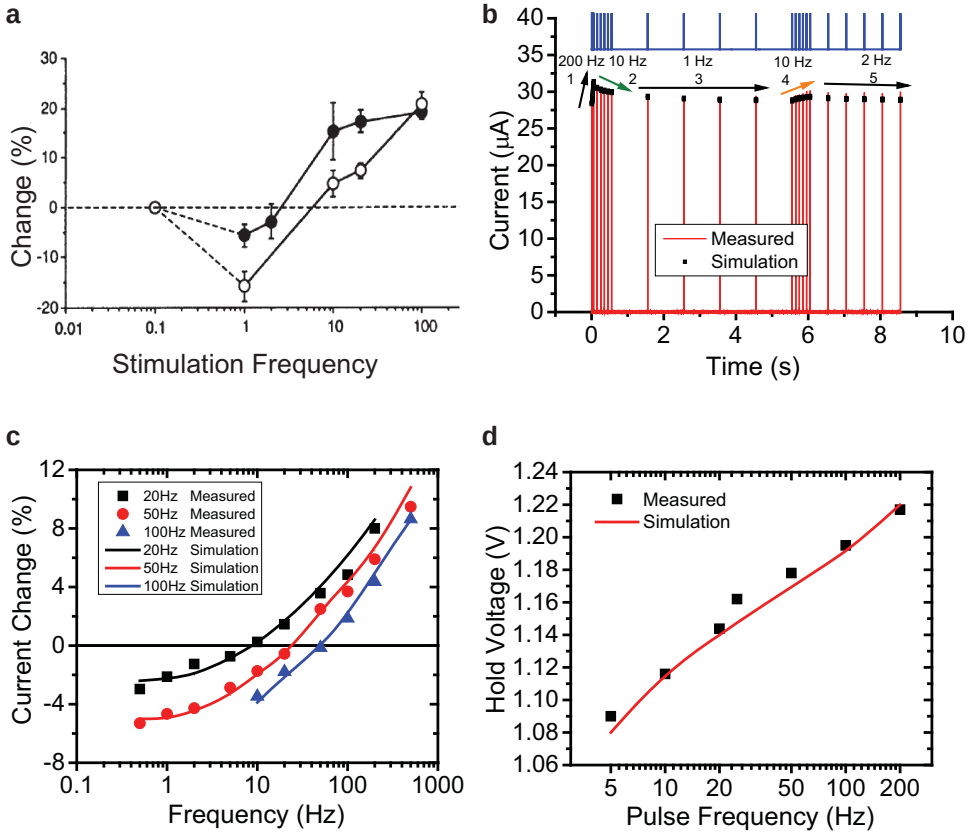

Figure 3. Activity dependent plasticity and sliding threshold effects in memristors. a) Relative change in synaptic weight as a function of stimulation frequency for two different cases. Low stimulation frequency results in depression and high stimulation frequency results in facilitation, and the threshold moves to lower frequency under the light-deprived condition (filled symbols) compared to the normal condition (open symbols). Data were obtained in rat visual cortex and reproduced with permission from ref. [42]. b) Memristor response to consecutive programming pulse trains (1 V, 1 ms, blue lines) at different frequencies. The 10 Hz pulse train caused current decrease in step 2 following strong stimulation in step 1, but current increase in step 4 following weak stimulation in step 3. Black squares: Simulation results from the memristor model using experimental parameters. c) Memristor current change as a function of the stimulation frequency after the memristor has been experienced to different levels of activities. Pulse trains consisting of five pulses (1.2 V, 1 ms) with different repetition frequencies were used to program the memristor. Black squares, red circles, and blue triangles represent experimental data. The solid lines are simulation results from the memristor model using experimental parameters. d) Measured threshold hold voltage as a function of previous activity (represented by different pulse frequency). The device was stimulated by pulse trains with the same repetition frequency of 50 Hz but different amplitudes. Black squares: Experimental data. Solid line: Simulation results from the memristor model using experimental parameters.

conditions shows that the effect of the stimulation for a memristor can also be dependent on previous activity.

The behavior observed in the WO_x memristors can be explained by the V_O dynamics of the memristor, as the conductance change is determined by the competition of the effects of the stimulation pulse and the decay of the state variables w_c and w_m. The experimentally observed experience-dependent behaviors can be fully reproduced in simulation based on the device model of Equations (2)–(4) (black squares, Figure 3b). Briefly, during the experiment in Figure 3b, the 200 Hz pulse train drove w_m to a high value which leads to small effective time constants $\tau_m^*(w_m)$ and $\tau_c^*(w_m)$ (Supporting Information) and enhanced decay of w_c and w_m in Equations (3) and (4). As a result, the subsequent 10 Hz pulse train was not sufficient to overcome the fast w_c decay and increase the memristor conductance anymore and an overall conductance drop was observed. On the contrary, after the 1 Hz pulse train, w_m has fully relaxed so the decay of w_c and w_m has slowed down significantly. As a result, the same 10 Hz pulse train afterward was enough to bring the conductance up. In other words, the same device can experience either conductance increase or decrease at a given stimulation condition, depending on the previous activity of the device.

With this understanding, we performed an experiment analogous to that of Bear et al.[42] (Figure 3a). In this study, we first experienced the device to one of three levels of activities by the application of ten pulses at either 10, 20, or 50 Hz, then five write pulses (1.2 V, 1 ms) with different repetition frequencies were applied and the net current changes (before and after the application of the write pulses) were recorded. The experiment is repeated by fully relaxing the device to the resting state (with w_c and w_m relaxed to their respective resting values), and the change in current during the five write pulses was plotted against the stimulation frequency of the write pulses, for the three cases. As shown in Figure 3c, a low stimulation frequency in general leads to conductance decrease (negative change)

due to the previous activities and a high frequency in general leads to conductance increase (positive change). Moreover, the threshold frequency at which the net conductance change is zero is observed to depend on the previous activities as well, as evidenced by the shift in the three curves corresponding to the three levels of activities the device has been subjected to. The threshold frequency will slide to the right (higher frequency) when previous activity is stronger, similar to the observations in neurobiology shown in Figure 3a. Importantly, these behaviors can be fully explained by the internal memristor dynamics using w_m and w_c as state variables, as evidenced by the quantitative agreement between experimental data and simulation results shown in Figure 3c.

The sliding threshold effect can be reflected as either a change in threshold frequency at the same stimulation amplitude, as observed in neurobiological studies and shown in Figure 3c, or a change in threshold amplitude at the same stimulation frequency. Both effects may be relevant for memristor devices and can be used in hardware-based neuromorphic systems. The sliding threshold amplitude effect is demonstrated in Figure 3d. In this study, the device again was first subjected to different levels of activities, then a pulse train consisting of five pulses with a fixed frequency (50 Hz) but different amplitudes was applied and the amplitude at which the device conductance can be maintained was recorded. As can be seen in Figure 3d, to maintain the device conductance at a given stimulation frequency, the threshold amplitude shifts to higher voltages with stronger previous activities. This behavior can be again quantitatively captured by the memristor model (solid line, Figure 3d).

2.4. Effect of Short-Term Dynamics on Long-Term State Change

More importantly, even though w_m is effective at short-term only, what the device experiences at short-time scales can have long-lasting effects and lead to long-term plasticity behavior. For example, PPF is a short-term effect and may be explained by evoking the short-term behavior only. However, different long-term states can also be achieved by controlling the pulse intervals during PPF measurements. To verify this, after a pair of stimulation pulses had been applied with different interpulse intervals, the device conductance was measured 5 s later to ensure that all short-term effects have fully decayed and the device has entered the long-term regime. **Figure 4**a plots the change in read current (current read 5 s after the stimulation minus the reference value read before the first stimulation pulse) versus the stimulation pulse interval. A larger conductance increase was still found for shorter stimulation intervals, suggesting the relative timing between the stimulation pulses also affect the long-term value of the state variable w_c long after all short-term effects have disappeared. This result can be explained with the aid of the second-order memristor model, as shown in Figure 4b. The state variable w_m was increased by the first pulse then decays following the fast time constant (blue lines). If the interval between the two pulses is small enough then at the moment when the second pulse arrives w_m is still elevated and causes a large change in the state variable w_c through Equation (4) (red solid line). On the other hand, if the interval between the pulses is long, w_m has already decayed to a very low value and the second pulse will only cause a small change in the state variable w_c (red dotted line). In this sense, w_m can be loosely considered as playing the role of (postsynaptic) Ca^{2+} concentration and provides an intrinsic timing and modulation mechanism in the model developed by Graupner and Brunel,[25] while w_c can be considered as the state variable that determines the synaptic weight.

2.5. Spike-Timing-Dependent Plasticity Achieved by Internal Ionic Dynamics

A key inference of Graupner and Brunel is that different synaptic learning rules may be explained in the same model framework of Ca^{2+}-dependent synaptic weigh change.[25] Below we show that the internal V_O dynamics can indeed also naturally lead to timing-based synaptic plasticity effects such as STDP.

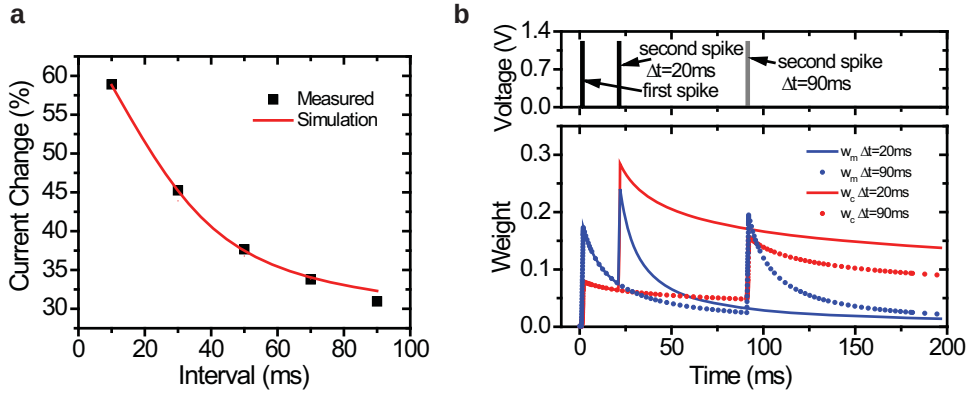

Figure 4. Effect of short-term behavior on long-term weight change. a) Changes in the memristor conductance measured 5 s after the application of a pair of programming pulses (1.4 V, 1 ms) versus the interval between the pulses. The differences in activity at short-term lead to measurable differences in long-term memristor weight. Black squares: Experimental data. Solid line: Simulation results from the memristor model using experimental parameters. b) Simulation results illustrating how the short-term behavior affected long-term weight change. The difference in long-term weight is caused by the different values of residue w_m at the moment when the second pulse is applied. State variable w_c and state variable w_m under two conditions (interval between two pulses Δt = 20, 90 ms) are shown.

Together with the rate-based learning (spike-rate-dependent plasticity, SRDP) shown in Figures 2 and 3, these results verify that the diverse STDP and SRDP synaptic characteristics at different experimental conditions can be well emulated by internal dynamics of memristors in a simple theoretical framework.

In STDP, the synapse is subjected to repetitive pre- and postsynaptic spike pairs, and the relative timing of the pre- and postsynaptic spikes determines whether the synaptic weight will be potentiated or depressed and by how much.[28] If presynaptic spike arrives before postsynaptic spike (pre–post pair), the pairs will cause potentiation while a reversed sequence (post–pre pair) will cause depression. Moreover, a larger time interval between the pre- and postsynaptic spikes will lead to smaller weight modification. Instead of relying on external factors that keep the timing information, in neurobiology, the relative timing information between the pulses is natively embedded, e.g., by the natural decay of Ca^{2+} levels which provides an internal timing mechanism.[24,25] Here, we demonstrate that STDP behaviors can be achieved in memristors with similarly simple, nonoverlapping pre- and postsynaptic spike pairs, and, similar to the case of biological synapses, STDP is achieved naturally since the relative timing information is encoded internally through the V_O dynamics, specifically, that of w_m.

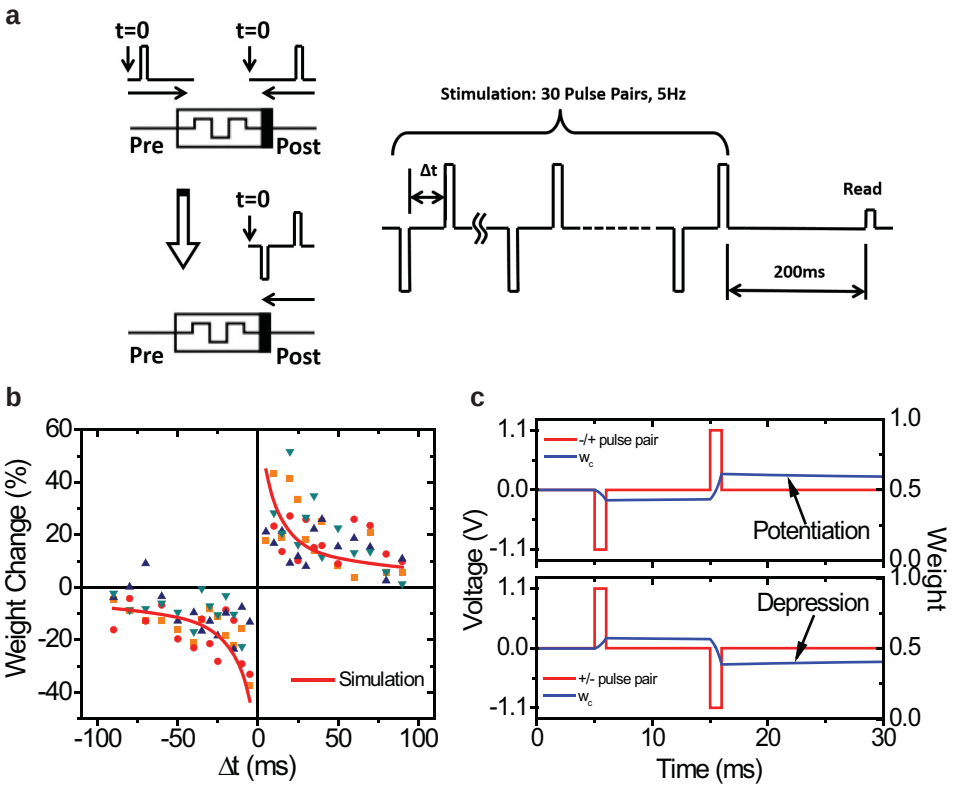

Figure 5. Implementation of spike-timing-dependent plasticity using the native V_O dynamics. a) Left: Experimental setup, a pre–post pair consisting of identical spikes is equivalent to a negative/positive pulse pair applied on the postsynaptic side; right: the pre–post programming protocol including 30 pulse pairs (–1.1 V, 1 ms/1.1 V, 1 ms) applied at 5 Hz for stimulation, followed by read 200 ms after stimulation. Post–pre pairs are applied similarly. b) Memristor weight change as a function of the relative timing between the pre- and postsynaptic pulses, $\Delta t = t_{post} - t_{pre}$. Symbols: Experimental results obtained from four different tests. Solid lines: Simulation results from the memristor model using experimental parameters. c) Simulation results illustrating how relative timing of the pulses affects memristor weight. Only w_c is shown here for clarity. The second pulse in the pair has a larger effect on w_c due to residue enhanced w_m from the first pulse, and can cause either potentiation or depression depending on the relative timing between the pre- and postsynaptic pulses.

The pulse pair we use contains a negative erase pulse (–1.1 V, 1 ms) representing the effect of a presynaptic spike and a positive write pulse (1.1 V, 1 ms) representing that of a postsynaptic spike, both applied at the postsynaptic side. This configuration is equivalent to applying identical, positive pulses on both the presynaptic and postsynaptic sides of the device as shown in **Figure 5**a. Before each test, the device was stimulated with the same pulse train consisting of ten positive pulses (1.2 V, 1 ms, 200 Hz). In each test, 30 pulse pairs of either positive–negative pulse pair (+/− pair, representing the post–pre spike condition) or negative–positive pulse pair (−/+ pair, representing the pre–post spike condition) were then applied at 5 Hz repetition frequency, as shown in Figure 5a, right side. The device conductance was measured 0.2 s after the last pair and compared to that of the reference value, which was measured at identical conditions but without the application of the pre–post or post–pre pairs. The device was then brought back to the same starting condition and the experiment was repeated for different pulse pair configurations. As shown in Figure 5b, for pre–post condition ($\Delta t > 0$), the memristor conductance increases while for post–pre condition ($\Delta t < 0$), the memristor conductance decreases. In other words, even though symmetric presynaptic (negative) and postsynaptic (positive) pulses were applied with identical amplitude and pulse width, their effects do not cancel each other and the net effect is found to be more strongly dominated by the effect of the second pulse. This observation can be understood again within the second-order memristor model, as illustrated in Figure 5c. Here, the state variable w_c after a positive–negative pulse pair shows a net decrease, since the erase effect of the second pulse will be stronger due to the residue enhanced value of w_m (which was enhanced by the first pulse). Detailed results of the modeling can be found in the Supporting Information. Similarly, the negative–positive pair leads to a net increase of the state variable w_c and a net increase of device conductance.

Moreover, since the enhancement effect of the second pulse is caused by the residue of the increased state variable w_m.

The amplitude of the enhancement is dependent on the relative timing Δt of the first (which enhances w_m) and the second pulse (which utilizes this enhancement) inside the pulse pair. Specifically, after the first pulse, the enhanced state variable w_m decays following a characteristic time constant τ_m^*, so a larger Δt between the two pulses leads to a smaller residue w_m and subsequently a smaller change in the state variable w_c during the second pulse, and a smaller measured conductance change. As a result, the accumulating net weight change of the pulse pairs, which is dominated by the second pulse in each pair, shows an inverse relationship with Δt. Indeed, an effect analogous to STDP was clearly observed, with larger relative timing between two pulses (larger Δt) resulting in smaller conductance change[28] and vice versa, as also shown in Figure 5b. Here again the state variable w_m plays the role of the (postsynaptic) Ca^{2+} concentration and provides an intrinsic timing mechanism, and in turn affects the plasticity of the weight state variable w_c. Similar to other experiments discussed earlier, the second-order memristor model can quantitatively explain the STDP behavior (solid lines, Figure 5b) with essentially only a single set of material-dependent parameters (Supporting Information).

3. Conclusions

We show that several important, rate- and timing-based synaptic behaviors at different time scales can be implemented using simple, biorealistic pulses in memristors naturally, by employing the internal ionic dynamics of the device. Following the theoretical framework based on Ca^{2+} driven synaptic plasticity, different synaptic behaviors including paired-pulse facilitation, frequency-dependent facilitation, sliding threshold effect, and timing-based plasticity (STDP) can be implemented and quantitatively explained using a second-order memristor model. We note that the memristor device and model still do not capture all the biological details. For example, in biology short-term plasticity is believed to be affected by presynaptic calcium concentration[27] and long-term plasticity is believed to be modulated by postsynaptic calcium concentration,[43] while only one calcium-like state variable w_m is employed in the device model to explain both short-term and long-term effects. However, the identification of the different state variables w_m and w_c and the effective roles played by them still allowed one to adopt the spirit of the calcium-concentration based theoretical framework to explain the different experimental results and guide further device and circuit developments. Specifically, we note that to emulate the synaptic behaviors in a biorealistic manner, two critical features need to be present: first, the device should exhibit analog resistance switching behavior, i.e., gradual conductance change during SET and RESET operations; second, there should exist an internal physical process that offers a short-term decay dynamics to enable activity-dependent conductance change. Looking toward the future, along with other recent studies,[26] not only will these findings enable the implementation of dynamic, adaptive neuromorphic systems in a biorealistic fashion, the wealth of knowledge already obtained at the atomic level regarding the physical processes inside memristors and the power of the memristor model based on a simple set of equations will stimulate the development of other second-order or even higher order memristive systems based on different types of physical mechanisms for efficient memory, computing, and other applications.

Supporting Information

Supporting Information is available from the Wiley Online Library or from the author.

Acknowledgements

The work at the University of Michigan was support by the AFOSR through MURI Grant No. FA9550-12-1-0038, by the National Science Foundation (NSF) through Award Nos. ECCS-0954621 and CCF-1217972, and by DARPA through Award No. HR0011-13-2-0015. The views expressed in this paper are those of the authors and do not reflect the official policy or position of the Department of Defense or the U.S. Government. Approved for public release. Distribution unlimited. The authors acknowledge S. Kim and S. Gaba for helpful discussions. The authors declare that they have no competing financial interests.

Received: April 9, 2015
Revised: May 8, 2015
Published online: June 1, 2015

[1] L. O. Chua, *IEEE Trans. Circuit Theory* **1971**, *18*, 507.
[2] L. O. Chua, S. M. Kang, *Proc. IEEE* **1976**, *64*, 209.
[3] D. B. Strukov, G. S. Snider, D. R. Stewart, R. S. Williams, *Nature* **2008**, *453*, 80.
[4] M. Di Ventra, Y. V. Pershin, L. O. Chua, *Proc. IEEE* **2009**, *97*, 1717.
[5] R. Waser, R. Dittmann, G. Staikov, K. Szot, *Adv. Mater.* **2009**, *21*, 2632.
[6] A. Sawa, *Mater. Today* **2008**, *11*, 28.
[7] D.-H. Kwon, K. M. Kim, J. H. Jang, J. M. Jeon, M. H. Lee, G. H. Kim, X.-S. Li, G.-S. Park, B. Lee, S. Han, M. Kim, C. S. Hwang, *Nat. Nanotechnol.* **2010**, *5*, 148.
[8] J. J. Yang, D. B. Strukov, D. R. Stewart, *Nat. Nanotechnol.* **2013**, *8*, 13.
[9] T. Chang, Y. Yang, W. Lu, *Circuits Syst. Mag. IEEE* **2013**, *13*, 56.
[10] D. Kuzum, S. Yu, H.-S. P. Wong, *Nanotechnology* **2013**, *24*, 382001.
[11] J. Borghetti, G. S. Snider, P. J. Kuekes, J. J. Yang, D. R. Stewart, R. S. Williams, *Nature* **2010**, *464*, 873.
[12] S. H. Jo, T. Chang, I. Ebong, B. B. Bhadviya, P. Mazumder, W. Lu, *Nano Lett.* **2010**, *10*, 1297.
[13] G. Snider, R. Amerson, D. Carter, H. Abdalla, M. S. Qureshi, J. Leveille, M. Versace, H. Ames, S. Patrick, B. Chandler, A. Gorchetchnikov, E. Mingolla, *Computer* **2011**, *44*, 21.
[14] T. Ohno, T. Hasegawa, T. Tsuruoka, K. Terabe, J. K. Gimzewski, M. Aono, *Nat. Mater.* **2011**, *10*, 591.
[15] M. Di Ventra, Y. V. Pershin, *Nat. Phys.* **2013**, *9*, 200.
[16] T. Chang, S.-H. Jo, K.-H. Kim, P. Sheridan, S. Gaba, W. Lu, *Appl. Phys. A* **2011**, *102*, 857.
[17] T. Chang, S.-H. Jo, W. Lu, *ACS Nano* **2011**, *5*, 7669.
[18] D. Kuzum, R. G. D. Jeyasingh, B. Lee, H.-S. P. Wong, *Nano Lett.* **2012**, *12*, 2179.
[19] F. Alibart, S. Pleutin, O. Bichler, C. Gamrat, T. Serrano-Gotarredona, B. Linares-Barranco, D. Vuillaume, *Adv. Funct. Mater.* **2012**, *22*, 609.
[20] P. Krzysteczko, J. Münchenberger, M. Schäfers, G. Reiss, A. Thomas, *Adv. Mater.* **2012**, *24*, 762.
[21] Z. Q. Wang, H. Y. Xu, X. H. Li, H. Yu, Y. C. Liu, X. J. Zhu, *Adv. Funct. Mater.* **2012**, *22*, 2759.

[22] C. Zamarreño-Ramos, L. A. Camuñas-Mesa, J. A. Pérez-Carrasco, T. Masquelier, T. Serrano-Gotarredona, B. Linares-Barranco, *Front. Neurosci.* **2011**, *5*, 26.
[23] S.-N. Yang, Y.-G. Tang, R. S. Zucker, *J. Neurophysiol.* **1999**, *81*, 781.
[24] H. Z. Shouval, M. F. Bear, L. N. Cooper, *Proc. Natl. Acad. Sci. U.S.A.* **2002**, *99*, 10831.
[25] M. Graupner, N. Brunel, *Proc. Natl. Acad. Sci. U.S.A.* **2012**, *109*, 3991.
[26] S. Kim, C. Du, P. Sheridan, W. Ma, S. Choi, W. D. Lu, *Nano Lett.* **2015**, *15*, 2203.
[27] R. S. Zucker, W. G. Regehr, *Annu. Rev. Physiol.* **2002**, *64*, 355.
[28] G. Bi, M. Poo, *J. Neurosci.* **1998**, *18*, 10464.
[29] R. Waser, M. Aono, *Nat. Mater.* **2007**, *6*, 833.
[30] J. P. Strachan, A. C. Torrezan, F. Miao, M. D. Pickett, J. J. Yang, W. Yi, G. Medeiros-Ribeiro, R. S. Williams, *IEEE Trans. Electron Devices* **2013**, *60*, 2194.
[31] D. B. Strukov, R. S. Williams, *Appl. Phys. A* **2008**, *94*, 515.
[32] W. M. Cowan, Thomas C. Südhof, Charles F. Stevens, *Synapses* 1st ed., The Johns Hopkins University Press, Baltimore, MD **2003**.
[33] A. Rozov, N. Burnashev, B. Sakmann, E. Neher, *J. Physiol.* **2001**, *531*, 807.
[34] R. Yang, K. Terabe, G. Liu, T. Tsuruoka, T. Hasegawa, J. K. Gimzewski, M. Aono, *ACS Nano* **2012**, *6*, 9515.
[35] Y. Y. Chen, M. Komura, R. Degraeve, B. Govoreanu, L. Goux, A. Fantini, N. Raghavan, S. Clima, L. Zhang, A. Belmonte, A. Redolfi, G. S. Kar, G. Groeseneken, D. J. Wouters, M. Jurczak, *Int. Electron Devices Meet.* **2013**, 10.1.1.
[36] Y. B. Nian, J. Strozier, N. J. Wu, X. Chen, A. Ignatiev, *Phys. Rev. Lett.* **2007**, *98*, 146403.
[37] I. Valov, E. Linn, S. Tappertzhofen, S. Schmelzer, J. van den Hurk, F. Lentz, R. Waser, *Nat. Commun.* **2013**, *4*, 1771.
[38] T. V. P. Bliss, G. L. Collingridge, *Nature* **1993**, *361*, 31.
[39] Y. V. Pershin, M. Di Ventra, *Proc. IEEE* **2012**, *100*, 2071.
[40] P. A. Salin, M. Scanziani, R. C. Malenka, R. A. Nicoll, *Proc. Natl. Acad. Sci. U.S.A.* **1996**, *93*, 13304.
[41] E. L. Bienenstock, L. N. Cooper, P. W. Munro, *J. Neurosci.* **1982**, *2*, 32.
[42] A. Kirkwood, M. G. Rioult, M. F. Bear, *Nature* **1996**, *381*, 526.
[43] R. Zucker, *Curr. Opin. Neurobiol.* **1999**, *9*, 305.